Silica deposition as an approach for improving the hydrothermal stability of an alumina support during glycerol aqueous phase reforming

Fang Liu[a], Chukwuemeka Okolie[b], Ryan M. Ravenelle[b], John C. Crittenden[c], Carsten Sievers[b,*], Pieter C.A. Bruijnincx[a,*], Bert M. Weckhuysen[a,*]

[a] Inorganic Chemistry and Catalysis, Debye Institute for Nanomaterials Science, Utrecht University, Universiteitsweg 99, 3584 CG Utrecht, The Netherlands
[b] Georgia Institute of Technology, School of Chemical & Biomolecular Engineering, 311 Ferst Dr. NW, Atlanta, GA 30332-0100, USA
[c] Georgia Institute of Technology, School of Civil & Environmental Engineering, 828 West Peachtree, Suite 320B Atlanta, GA 30332-0595, USA

ARTICLE INFO

ABSTRACT

Silica deposition on the benchmark aqueous phase reforming (APR) catalyst Pt/γ-Al$_2$O$_3$ is studied to prevent or limit hydrolytic attack of the support under hydrothermal APR conditions, for which boehmite formation by support hydration is a known cause for catalyst deactivation. Tetraethyl orthosilicate (TEOS) is employed as a silicon source in a straightforward liquid-phase, silylation process followed by catalyst calcination and reduction. Characterization by X-ray diffraction, temperature-programmed desorption of NH$_3$, infrared, ^{27}Al nuclear magnetic resonance and X-ray photoelectron spectroscopy of the fresh catalysts suggests that silica addition occurs preferentially on the support surface, resulting in weak Brønsted acid sites as well as in the formation of Si-O-Al linkages at the expense of specific surface Lewis acid sites. Silylation and calcination of Pt/γ-Al$_2$O$_3$ causes partial blockage of the metal surface area (12% loss), whereas γ-Al$_2$O$_3$ surface silica modification prior to Pt deposition makes controlled metal deposition difficult. Catalytic performance tests show the overcoated samples to be active in the APR of 5 wt% glycerol, albeit with lower H$_2$ production rates compared to the benchmark catalyst. Characterization of spent APR catalysts clearly demonstrates that silylation/calcination treatments effectively slows down the transformation of the γ-Al$_2$O$_3$ support due to the formation of a Si-O-Al interface. Overall, the lifetime of the catalyst is increased three-fold as a result of the surface overcoating treatment, with repetitive recycling ultimately leading to loss of the protective silica layer.

1. Introduction

The unsustainable consumption of fossil fuel reserves and continuously increasing energy demands are big challenges currently faced by our society [1–3]. Alternative and efficient routes for the production of energy and chemicals from sustainable resources, such as biomass, are therefore needed. Biomass can serve as a source of renewable hydrogen, a clean energy carrier but also a key reagent for the chemical industry. As a result, hydrogen production from glycerol via so-called aqueous phase reforming (APR) has received considerable attention [4–8]. Glycerol has been identified as an attractive biomass-derived feedstock being produced in large amounts as a by-product of biodiesel production [9–11]. Compared to more conventional hydrogen production routes, such as steam reforming, partial oxidation and autothermal reforming, APR is usually operated at a relative low temperature in a single reaction step. Under these conditions, the water-gas shift reaction is thermodynamically favourable, resulting in efficient H$_2$

production and a lower CO concentration in the product stream [11,12].

A large variety of (supported) metal-based catalysts, including Raney Ni, noble and non-noble metals on oxidic and carbon supports, have been used for hydrogen production by APR from glycerol and other oxygenated, renewable substrates [13–17]. Pt/γ-Al$_2$O$_3$ is commonly used as APR catalyst [14,18], showing good activity, high H$_2$ selectivity and limited alkane formation, albeit that this catalyst is unstable under the applied hydrothermal conditions [19,20]. It has been demonstrated that supported metal particles can suffer irreversible sintering under the high temperature and pressure conditions often applied in biomass reactions [20]. Besides, under APR conditions, oxidic supports such as γ-alumina can be hydrated, leading to phase changes in the support and, as a result, deactivation [21,22]. The γ-alumina in Pt/Al$_2$O$_3$ is well-known to transform into boehmite under typical APR conditions. For example, Ravenelle et al. [23] demonstrated that bare γ-Al$_2$O$_3$ was rehydrated in hot water and completely

converted into crystalline boehmite within 10 h with a significant loss of surface area. During this structural modification, supported metal particles can loose contact with their original binding sites leading to sintering or encapsulation, both of which are detrimental for catalyst activity [23]. Previous studies suggested this transformation to start with hydrolytic attack of the Lewis acid sites of the alumina support [24,25]. Indeed, supported metal particles as well as biomass-derived oxygenates in the reaction solution were reported to have a beneficial effect [26,27] on catalyst stability by "capping" specific, coordinatively unsaturated surface Al atoms. For example, Copeland et al. found that biomass-derived polyols can block Lewis acidic Al sites of γ-Al$_2$O$_3$ by formation of multidentate alkoxy surface species that protect the alumina from hydrolytic attack [25]. Similarly, Absi-Halabi et al. [28] proposed the improved hydrothermal stability of γ-Al$_2$O$_3$ in acetic acid solution to be related to the formation of acetate bridges by alumina acetylation, again emphasizing the protection of such primary rehydration sites as the reason for improved hydrothermal stability.

Various other approaches to γ-alumina support stabilization have been reported, including stabilization by doping with a broad range of other materials. For example, ConocoPhillips studied the use of dopants, such as silicon, cobalt, magnesium and others, to enhance the hydrothermal stability of alumina-supported catalysts for Fischer–Tropsch synthesis [29,30]. Byrd et al. [31] reported that the stability of γ-Al$_2$O$_3$ treated in supercritical water at 500 °C could be improved by inclusion of CeO$_2$. Alternatively, catalyst surface coating can also be used to limit or preclude the phase transformation process to boehmite. Pham et al. [32] deposited a thin, sucrose-derived carbonaceous layer on fumed alumina and demonstrated that the carbon coating led to improved thermal stability. Similarly, it was reported that the formation of a graphitic carbon layer on pelletized γ-alumina by chemical vapor deposition of methane can enhance catalyst thermal stability significantly [33].

Silylation of metal oxide surfaces has also emerged as a promising route to tune the surface properties of inorganic materials, such as silica, zeolites and alumina [34–36]. Zapata et al. [37] reported that hydrophobization of HY zeolites by functionalization with organosilanes could protect the material from structural collapse in hot liquid water due to increased hydrophobicity. In case of γ-Al$_2$O$_3$, silylation followed by high temperature calcination could block the surface Lewis acid Al sites that serve as initial hydration sites for boehmite formation via coordinative saturation and the formation of Al−O−Si bonds, inhibiting water adsorption [36]. Here, we explore surface silylation of Pt/ γ-Al$_2$O$_3$ with tetraethylorthosilicate (TEOS) followed by calcination as a means of protecting the support against hydrolytic attack to ultimately increase the stability of the catalyst under glycerol APR conditions. Recycle tests show that the silica deposition does indeed reduce boehmite formation and extends the catalyst lifetime, but cannot prevent eventual deactivation by dehydration entirely.

2. Experimental

2.1. Catalyst preparation

The 1 wt.% Pt/γ-Al$_2$O catalyst was prepared via wet impregnation. A slurry of H$_2$Pt(OH)$_6$ (99.9% metals basis, Alfa Aesar) and commercial γ-Al$_2$O$_3$ (3 μm APS powder, 99.97% metals basis, Alfa Aesar) was stirred at 40 °C for 24 h. The catalysts were dried at 110 °C under vacuum overnight and calcined right after at 500 °C with a heating ramp rate of 1 °C/min for 4 h (starting from room temperature) under a 20% O$_2$/N$_2$ flow. Prior to the silylation treatment, the catalyst was reduced in 10% H$_2$/N$_2$ flow at 300 °C (ramp rate 5 °C/min) for 3 h (starting from room temperature).

The silylation procedure was performed according to a literature protocol [38]. In a typical experiment, a mixture of 2.4 g tetraethyl orthosilicate (TEOS, 98% Alfa Aesar), 30 g ethanol, 8 g milli-Q water and 1 g of 1 wt.% Pt/Al$_2$O$_3$ was stirred at 40 °C for the designated time.

The quantity of precursor added corresponded to a theoretical loading of 40% silicon by weight (if all silicon was deposited). The solid was collected by centrifugation at 5000 rpm for 10 min and washed three times with ethanol, followed by drying at 60 °C and then 120 °C overnight, respectively. Prior to catalytic activity experiments, the samples were calcined and reduced under the conditions mentioned above. The effect of silylation time on catalyst performance was tested by using three different silylation times of 4 h, 8 h and 12 h and the obtained catalyst materials named as Pt/Al$_2$O$_3$-4, Pt/Al$_2$O$_3$-8 and Pt/Al$_2$O$_3$-12, respectively.

One additional reference catalyst, Pt/Al$_2$O$_3$-8R, was prepared in a reverse order compared to Pt/Al$_2$O$_3$-8 sample. The support alumina was first silylated for 8 h under conditions otherwise identical to the silylation procedure for the Pt/Al$_2$O$_3$-8 sample, followed by calcination and reduction. Subsequently, the wet impregnation method described above was employed to prepare 1 wt.% Pt/Al$_2$O$_3$-8R with the pre-modified alumina as support. Subsequent calcination and reduction conditions were again identical to those used in the preparation of Pt/Al$_2$O$_3$-8.

2.2. Catalytic activity test

Aqueous phase reforming (APR) of a 5 wt.% glycerol solution was performed in a 40 mL stainless Parr batch autoclave equipped with a back-pressure regulator and magnetic stirrer. In a typical experiment, 300 mg of catalyst and 10 g of the 5 wt.% glycerol solution were loaded into the reactor and the system was pressurized to 30 bar with helium. The reaction mixture was then heated to 225 °C and reacted for 12 h. An online dual channel micro-GC (Varian CP4900) equipped with thermal conductivity detector was employed to analyse the gas phase composition. A COX column with back flush was used for quantification of the gases and N$_2$ was added as internal standard. The composition of the liquid phase was measured using a Shimadzu 2010A GC with flame ionization detector. Spent catalyst was collected by filtration using a 0.45 μm Nylon filter membrane, followed by ethanol washing and drying. Glycerol conversion (X), yield (Y) and selectivities (S) of liquid phase products and H$_2$ are defined as follows:

$$X_{gly} (\%) = \frac{C_{0,gly} - C_{t,gly}}{C_{0,gly}} \times 100\% \tag{1}$$

$$Y_{t,i} (\%) = \frac{C_{t,i}}{C_{0,gly}} \times \frac{M_i}{M_o} \times 100\% \tag{2}$$

$$S_{t,i} (\%) = \frac{C_{t,i}}{C_{0,gly} - C_{t,gly}} \times \frac{M_i}{M_o} \times 100\% \tag{3}$$

$$S_{H_2} (\%) = \frac{n_{H_2}}{X_{gly} \times n_{gly}} \times \frac{1}{7} \times 100\% \tag{4}$$

Where $C_{0,gly}$ is initial glycerol concentration, $C_{t,gly}$ is glycerol concentration at time t, $C_{i,gly}$ is the concentration of product i at time t, M_o and M_i are the moles of carbon in glycerol and product i, respectively, n_{H2} and n_{gly} are the moles of H$_2$ produced and initial moles of glycerol, respectively.

For the recycle tests, the spent catalyst was retrieved after a standard run, rinsed, dried at 60 °C overnight and reused directly without any regeneration step. All (recycle) runs were carried out at 225 °C for 12 h under 30 bar of He. The recovery of each catalyst after every run was close to 100% and the amount of glycerol in every subsequent run was scaled to the amount of catalyst recovered with the constant total reaction weight (10 g) to allow for a proper comparison of the runs, the H$_2$ production rates were normalized to the intake of the recycled catalysts.

2.3. Characterization

X-ray diffraction (XRD) patterns measured using on a Bruker-AXS

D2 Phaser powder X-ray diffractometer using Co $K_{\alpha1,2}$ with $\lambda = 1.79026$ Å. Measurements were carried out between 10–85° 2θ using a step size of 0.04° and a scan speed of 1 s. Part of the patterns were recorded with Cu Kα radiation with an incident angle ranging from 2θ = 5–70° with a step size of 0.02° with a scan speed of 1 s.

Scanning transmission electron microscopy (STEM) and energy dispersive X-ray (EDX) analyses were conducted with a JEOL 100CX microscope at a 100 kV acceleration voltage. The samples were prepared by applying three drops of a catalyst in ethanol slurry onto a graphene-coated, 200 mesh copper grid. The slurry was homogenized using sonication prior to applying to the sample grid.

Pt loading was determined using an inductively coupled plasma optical emission spectrometry (ICP-OES). Sample were prepared by dissolving 100 mg of the catalyst samples in aqua regia at 90 °C overnight. After evaporation of the aqua regia at 160 °C, the samples were dissolved in 20 mL HCl at 90 °C. The silicon content analysis was performed by Mikroanalytisches Laboratorium Kolbe (Mikrolab Kolbe), Germany.

Hydrogen chemisorption experiments were performed on a Micromeritics ASAP 2020 instrument. The catalyst was reduced at 250 °C for 2 h. After reduction, the sample was degassed for 1 h at 250 °C. The sample was then cooled to 40 °C at which the H_2 adsorption isotherm was measured. The same procedure was applied for measurements with the spent recycled overcoated catalysts. A H_2/Pt stoichiometric ratio of 0.5 was used to calculate the metal dispersion. The metallic surface area was calculated by dividing the amount of surface platinum atoms (determined from the amount of hydrogen adsorbed) by the area density of surface platinum. The particle size d was determined using the equation below:

$$d = \frac{6}{s} \times \rho$$

where s = metallic surface area per gram of metal, ρ = density of the metal [39].

Solid-state ^{27}Al magic angle spinning (MAS) nuclear magnetic resonance (NMR) spectra were taken using a Bruker AV3 400 solid spectrometer. A high MAS rate of 12 kHz and a high magnetic field of 9.4 T helped to ensure that the spectra were quantitatively reliable. The samples were packed into a 4 mm zirconia rotor. A π/12 pulse was used for excitation, and a recycling delay of 250 ms was used. For each spectrum, a minimum of 2400 scans was recorded. The fractions of tetrahedrally and octahedrally coordinated Al nuclei were obtained by fitting the spectra using dmfit [26].

Thermal gravimetric analysis (TGA) was performed using a Perkin–Elmer Pyris 1 apparatus. 15 mg of catalyst sample was heated with a ramp of 5 °C/min to 850 °C in a 10 mL/min air flow.

Temperature programmed desorption of ammonia (NH_3-TPD) measurements were measured using a Micromeritics ASAP 2920 apparatus. First, about 100 mg of sample was dried in situ using a He flow of 10 cm^3/min with a temperature ramp of 5 °C/min up to 600 °C. Subsequently, the sample was cooled to 100 °C, at this point, NH_3 was fed at 25.3 cm^3/min. The sample was then heated to 600 °C with a ramp of 5 °C/min to induce desorption of NH_3. The desorbed NH_3 was quantified using a thermal conductivity detector (TCD). A cold trap was used to prevent water passing through the TCD.

N_2 physisorption isotherms were measured to determine surface areas and pore volumes using a Micromeritics Tristar 3000 setup. The samples were outgassed at 150 °C overnight under a N_2 flow prior to performing the measurements at liquid nitrogen temperature. Surface areas were determined using the Brunauer−Emmett−Teller (BET) theory.

Fourier-transform infrared (FT-IR) spectra in transmission mode were measured using a Perkin-Elmer 2000 instrument. Approximately 15 mg of the catalyst were pressed in to a self-supported pellet and placed into a well-sealed cell with CaF$_2$ window. The wafer was first activated at 500 °C (5 °C/min) for 1 h under high vacuum (10^{-6} mbar).

Subsequently, the cell was cooled down to 150 °C to record the spectra. After that, the sample was dosed with excess pyridine vapor, followed by high vacuum evacuation for 40 min. Literature values were used for the integrated molar extinction coefficients for quantitative determination of the Brønsted acid and Lewis acid site contents [40].

The X-ray photoelectron spectroscopy (XPS) measurements were carried out on a Thermo Scientific K-Alpha spectrometer, equipped with a monochromatic small-spot X-ray source and a 180° double-focusing hemispherical analyzer with a 128-channel detector. Spectra were obtained using an aluminum anode (Al Kα = 1486.6 eV) operating at 72 W and a spot size of 400 μm; samples were not handled under an inert atmosphere and should be considered passivated. Survey scans were measured at constant pass energy of 200 eV and region scans at 50 eV. The background pressure of the UHV chamber was 2×10^{-8} mbar.

3. Results and discussion

3.1. Catalyst characterization

To improve the hydrothermal stability of a benchmark 1 wt.% Pt/Al_2O_3 APR catalyst, the material was silylated with TEOS according to the method of Sato et al.[38] using three different silylation times (4, 8 and 12 h), followed by calcination and reduction. It was previously shown that the deposited silicon content was proportional to the amount of TEOS charged, resulting in reported weight loadings of 3.8–15.6 wt.% silicon on alumina [38]. The physicochemical properties of the overcoated materials are summarized in Table 1. XPS analysis showed the near-surface silicon (Si) loading in Pt/Al_2O_3-4, 8 and 12 to be 6.2, 18.0 and 33.7 wt.%, respectively. The steady increase with increased silylation time occurred as expected. On the other hand, ICP-OES analysis of the Pt/Al_2O_3-4, 8 and 12 samples showed bulk Si loadings of 1.1, 2.2 and 2.6 wt.%, respectively. Taken together, the results suggest preferential deposition of silica on the surface. The lower silicon loading compared to previous report might be due to the lower surface area of the γ-alumina used here [38]. To investigate the effect of the sequence of synthesis steps, one reference catalyst, Pt/Al_2O_3-8R, was also prepared with the silylation and calcination steps preceding Pt deposition. ICP-OES analysis showed that the Si loading in Pt/Al_2O_3-8R was 1.0 wt.%, which is surprisingly lower than Pt/Al_2O_3-8.

No obvious differences were seen in the XRD diffractograms of the freshly reduced catalyst before and after silylation, calcination and reduction indicating that the deposited silica layer was insufficiently

Table 1
The physicochemical properties of the catalysts before and after silica deposition.

Catalyst	Pt/Al$_2$O$_3$	Pt/Al$_2$O$_3$-4	Pt/Al$_2$O$_3$-8	Pt/Al$_2$O$_3$-12	Pt/Al$_2$O$_3$-8R
Pt loading [a] (wt.%)	0.83	0.76	0.71	0.68	1.0
Si content [a] (wt.%)	ND	1.1	2.1	2.6	1.0
Si content [b] (%)	ND	6.2	18.0	33.7	ND
Metal dispersion [c] (%)	30.9	31.7	27.0	29.5	21.1
Metallic surface area [c] (m^2/g)	0.63	0.59	0.47	0.49	0.43
Pt particle size [c] (nm)	3.7	3.6	4.2	3.8	5.4
Pt particle size [d] (nm)	1.3	ND	1.5	ND	2.8
BET surface area [e] (m^2/g)	64	57	59	58	60
Acid concentration [f] (mmol/g)	0.35	0.30	0.27	0.18	0.25

[a] ICP-OES.
[b] XPS.
[c] H$_2$ chemisorption.
[d] TEM.
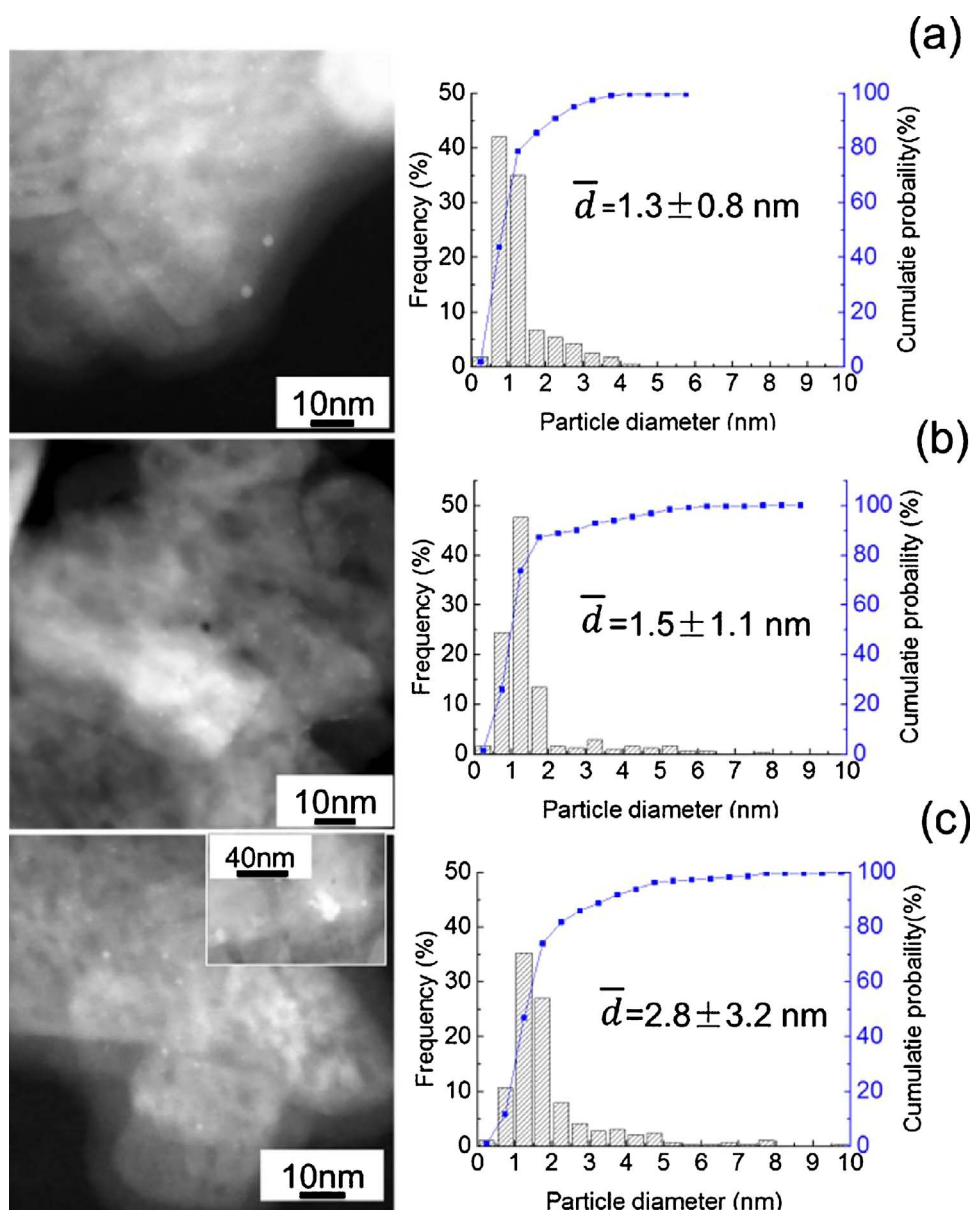[e] N$_2$ physisorption.
[f] TPD-NH$_3$.

Fig. 1. STEM images and metal particle size distributions of fresh (a) Pt/Al_2O_3, (b) Pt/Al_2O_3-8 and (c) Pt/Al_2O_3-8R.

thick to cause Bragg diffraction (Fig. S1). STEM analysis showed that the platinum nanoparticles were highly dispersed on the parent Al_2O_3 support, with an average particle size of 1.3 ± 0.8 nm (Fig. 1). After silylation, calcination and reduction, the particle size in Pt/Al_2O_3-8 increased slightly to 1.5 ± 1.1 nm, indicating that the mean metal particle sizes in the catalysts before and after surface treatment are very similar, which is in line with the H_2 chemisorption data (Table 1). A 12% decrease in accessible metal surface area was observed for sample that was treated for 8 h, and there was little change in metal surface area when the silylation time was increased to 12 h, showing that silica overcoating only leads to a limited reduction in accessible platinum surface area. As the particle size distribution did not change upon surface modification as seen by STEM (Fig. 1), the drop in accessible Pt surface area is attributed to partial coverage by the deposited siliceous species. One could envision that metal impregnation after overcoating would prevent such blockage of active metal surface area, but for Pt/Al_2O_3-8R, some large, agglomerated metal particles were observed (Fig. 1). The larger particle size and the lower accessible metal surface area seen for Pt/Al_2O_3-8R showed that Pt dispersion is more difficult to control on the pre-modified support than on pure alumina. Similarly, studies have shown some difficulty in controlling Pt dispersion on a

SiO_2 support. Lin et al. reported, for example, a bimodal Pt particle size distribution (1–1.5 and 4–7 nm) for SiO_2 supported catalysts, whereas Pt/Al_2O_3 showed a unimodal Pt size distribution with a mean size of 1.5 nm [41].

The BET surface area dropped slightly as expected from $64 \, m^2/g$ for the non-modified sample to $57\text{-}59 \, m^2/g$ after silica deposition. Surface silica modification of γ-Al_2O_3 before metal deposition led to an initial decrease in surface area from $70 \, m^2/g$ to $61 \, m^2/g$, after which Pt impregnation led to little further change.

The ^{27}Al MAS NMR spectra of the catalysts before and after treatment are shown in Fig. 2. The ^{27}Al MAS NMR spectrum of Pt/Al_2O_3 shows the typical resonances at 8 ppm and 65 ppm, attributed to octahedrally and tetrahedrally coordinated aluminum species, respectively [23]. Expectedly, surface overcoating followed by precursor decomposition did not lead to obvious differences in the ^{27}Al MAS NMR spectrum. No peaks corresponding to pentahedrally coordinated aluminum species were observed, indicating that silica deposition leads to a surface modification only, rather than the formation of any detectable (bulk) silica-alumina phases [42].

The effect of overcoating treatment on the total acidity of the catalyst materials, as determined by TPD-NH_3, is compared in Fig. S2. One
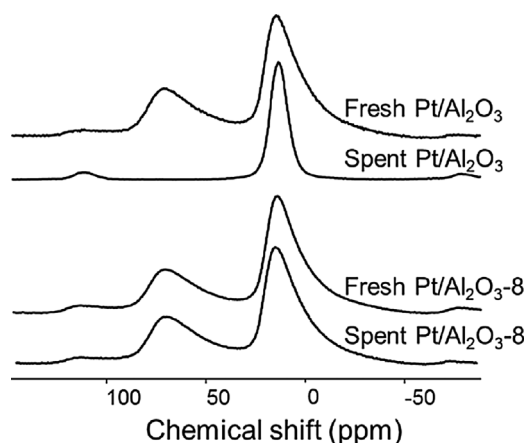
Fig. 2. ^{27}Al NMR spectra of a Si-free catalyst and a catalyst modified by silylation, calcination and reduction before (fresh) and after (spent) APR.
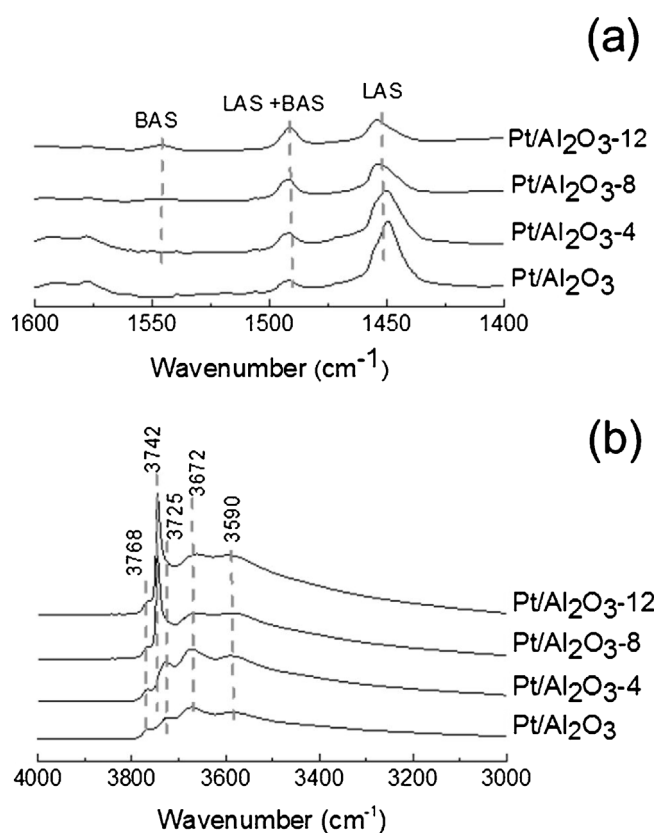

Fig. 3. (a) FT-IR spectra after pyridine adsorption of all catalysts, (b) OH region of the FT-IR spectra of fresh catalysts before and after silica modification.

Table 2
Acid site concentration as measured by Pyridine-FT-IR spectroscopy.

Catalyst	Acid site concentrations (µmole/g)		
	C$_{total}$	Brønsted	Lewis
Pt/Al$_2$O$_3$	618	0	618
Pt/Al$_2$O$_3$-4	575	0	575
Pt/Al$_2$O$_3$-8	365	35	330
Pt/Al$_2$O$_3$-12	232	59	173

broad peak of NH$_3$ desorption was observed in all samples. The maxima located at ~280 °C can be assigned to weak and medium strength acid sites [43]. Acid site concentration (Table 1) decreased with increasing

modification time, similar to previous observations of selective consumption of the strong Al Lewis acid sites upon exposure to TEOS [44]. Pyridine adsorption followed by IR spectroscopy indicated that only Lewis acid sites (LAS) were present in the parent Pt/Al$_2$O$_3$ catalyst (Fig. 3a). However, silica deposition led to a decrease in Lewis acidity, with only about 25% of the LAS remaining in Pt/Al$_2$O$_3$-12. On the other hand, Brønsted acidic sites (BAS) were detected for 8 or 12 h overcoated samples, as evidenced by the appearance of the vibration at around 1545 cm^{-1} that is characteristic BAS [45]. Regardless of BAS formation, the total acid site concentration of the overcoated samples dropped significantly upon modification (Table 2), in line with the NH$_3$-TPD results.

The OH region of the FT-IR spectrum of Pt/Al$_2$O$_3$ (Fig. 3b) shows 4 distinct peaks, corresponding to different coordination environments of the OH groups [46]. The peaks at 3765, 3725 and 3672 cm^{-1} were assigned to terminal, doubly-bridged and triply-bridged OH groups, respectively. The broad peak at 3590 cm^{-1} has been attributed to hydrogen-bonded OH groups [47,48]. Upon modication with TEOS, a sharp peak centered at 3742 cm^{-1} appeared, attributed to isolated silanols, considered to be Brønsted acid sites [44,49]. The IR spectra of Pt/Al$_2$O$_3$-8 and 12 showed a decrease in intensity of the absorption bands at 3672 and 3725 cm^{-1} compared to pristine Pt/Al$_2$O$_3$, suggesting that surface unsaturated Al atoms were consumed in the overcoating process. No obvious C–H vibrations were observed in the region of 2800–3000 cm^{-1} of any of the spectra (Fig. S3), indicative of complete decomposition of TEOS during calcination [50]. Given the change in catalyst acidity before and after modification, it can be inferred that Al-O-Si linkages were formed successfully at the expense of specific surface Lewis acid sites, which serve as original hydration sites for the undesired conversion to boehmite. Similarly, Mouat et al.[44] suggested that TEOS modification of an γ-alumina surface preferentially occurs on strong Lewis acid sites, also observing the formation of "mild" Brønsted acid sites. As stated above, silica deposition was hypothesized to inhibit water adsorption of Al$_2$O$_3$ by Al coordinative saturation of unsaturated Al species and the formation of Al–O–Si bonds, with the characterization data now suggesting that improved stability under hydrothermal conditions can indeed be anticipated.

3.2. Catalyst performance in glycerol APR

The effect of the silica overcoating treatment on catalyst performance, in particular stability, was then assessed in the APR reaction of pure glycerol. Standard reaction conditions entailed 12 h runs of a 5 wt. % aqueous glycerol solution at 225 °C. Catalyst performance was compared in a semi-batch reactor setup, which allows for an initial assessment of activity and, upon catalyst recycling, possible catalyst deactivation [51,52]. As shown above, catalyst synthesis using silica overcoating prior to metal impregnation made controlled Pt deposition difficult and the Pt/Al$_2$O$_3$-8R sample was therefore not included in the APR tests. Fig. 4a shows glycerol conversion as function of time over the catalysts before and after modification. The Pt/Al$_2$O$_3$ catalyst had 100% conversion of glycerol in 5 h of reaction time. Overcoated catalysts were slower to convert glycerol, and conversion decreased with increasing modification time. For the Pt/Al$_2$O$_3$-4 and Pt/Al$_2$O$_3$-8 samples, glycerol was converted completely after roughly 7 h and 11 h, respectively, whereas after 12 h 23% glycerol had not reacted over the Pt/Al$_2$O$_3$-12 catalyst.

The liquid phase composition was determined as function of time by HPLC analysis (Fig. 5 and Table S1). The same products and intermediates were observed for non-modified and modified catalysts, including lactic acid (LA), acetic acid (AA), ethylene glycol (EG), hydroxyacetone (HA), 1,2-propanediol (1,2-PD), acetaldehyde (Ac) and ethanol (EtOH). Overall, the total amount of liquid products increased upon surface modification and as a function of modification time. For instance, the yields of liquid products for Pt/Al$_2$O$_3$ and Pt/Al$_2$O$_3$-4, 8, 12 were 11%, 16%, 24% and 29%, respectively, at ~60% glycerol
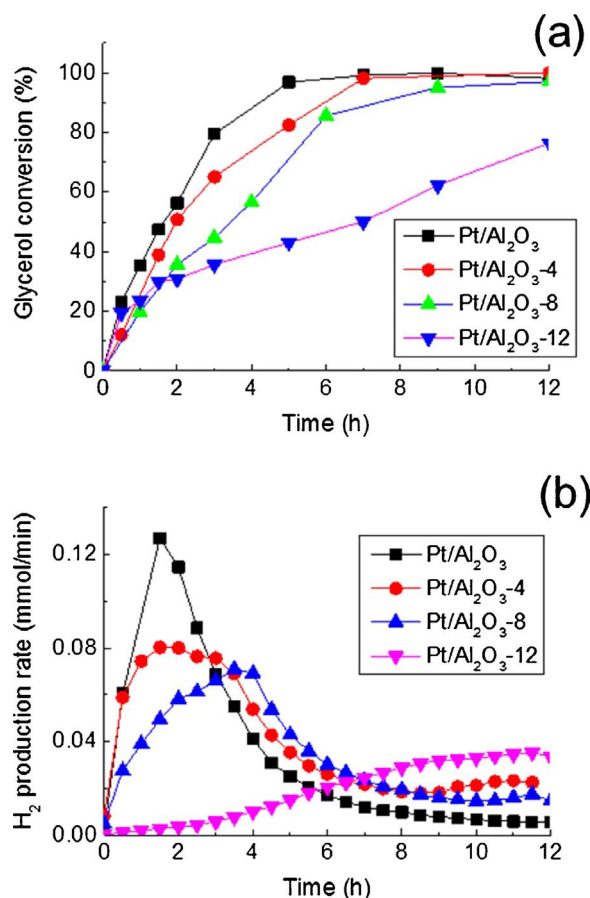
Fig. 4. (a) Glycerol conversion and (b) H_2 production rate as a function of time for overcoated and non-modified Pt/Al_2O_3.

conversion. Among those liquid products, the amount of HA and 1,2-PD increased significantly as a function of modification time. In particular, the selectivity to HA was eight times higher for the 12 h treated sample than the non-modified sample due to the increased Brønsted acidity of the silica-containing samples. Online gas phase analysis showed the expected formation of H_2 and CO_2, as well as some minor amounts of methane (Fig. S4). Only trace amounts of CO were detected in all experiments, illustrative of efficient water-gas shift activity (Fig. S4). Fig. 4b shows the H_2 production rate as function of reaction time over the bare and overcoated fresh catalysts, with hydrogen formation clearly decreasing with increasing modification time. The H_2 selectivity of Pt/Al_2O_3-4 was 73%, which is comparable to that of parent catalyst (72%). However, longer treatment time resulted in a drop in H_2 selectivity to 66% and 47% for Pt/Al_2O_3-8 and 12 samples. This decreased selectivity for H_2 agrees with the increase in production of liquid products.

H_2 production requires high reforming and water-gas shift activities, with the initial step being the dehydrogenation of glycerol to generate glyceraldehyde/pyruvaldehyde, followed rapid C−C bond cleavage by decarbonylation (Fig. S5) [53]. Dehydration reactions and reactions consuming hydrogen, such as the transformation of glycerol to 1,2-propylene glycol by acid-catalyzed dehydration to hydroxyacetone followed by hydrogenation, should be avoided [54,55]. Obviously, higher selectivity towards HA and 1,2-PD leads to lower H_2 production as they are the products formed by an initial dehydration rather than dehydrogenation step [55]. Of course, Brønsted acid sites play a key role in promoting such dehydration reactions [56]. In our case, silica deposition resulted in the generation of Brønsted acid sites at the expense of Lewis acid sites, causing the increase in undesired dehydration side reactions, hindering H_2 production with the overcoated samples.

The spent catalysts were characterized by XRD, ^{27}Al NMR, thermal gravimetric analysis (TGA), STEM and N_2 physisorption to better understand the impact of surface silica deposition on the support layer stability of the catalyst during the APR reaction.

As expected, after 12 h of APR, Pt/Al_2O_3 catalyst was fully converted to boehmite. Fig. 6 shows the sharp diffraction peaks at
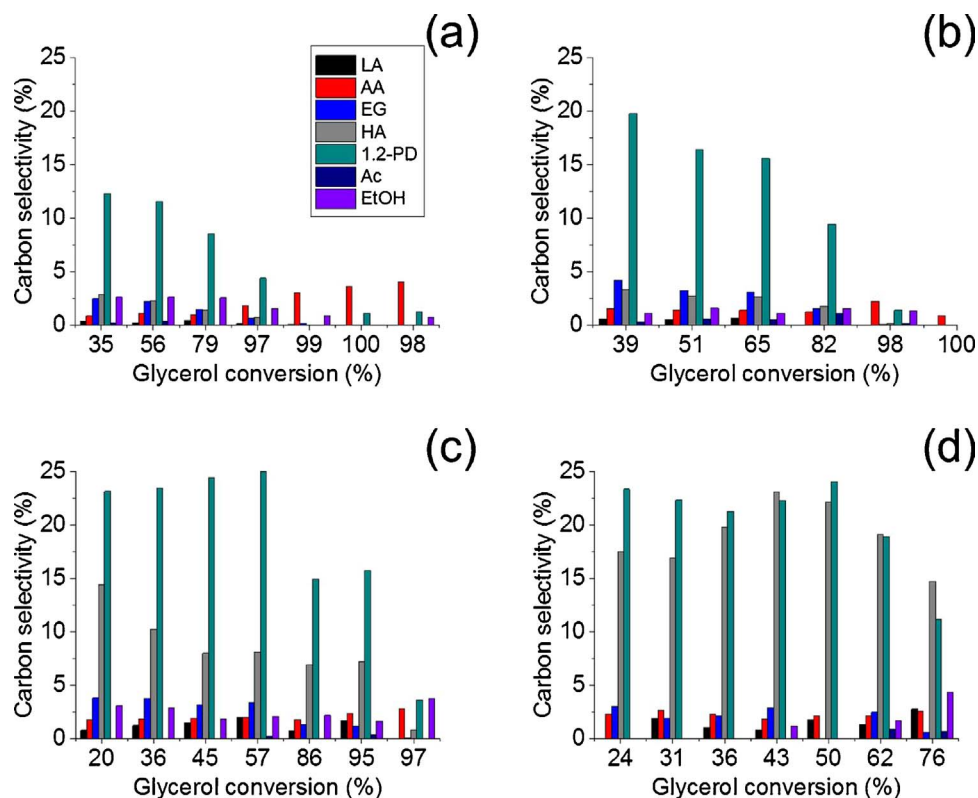

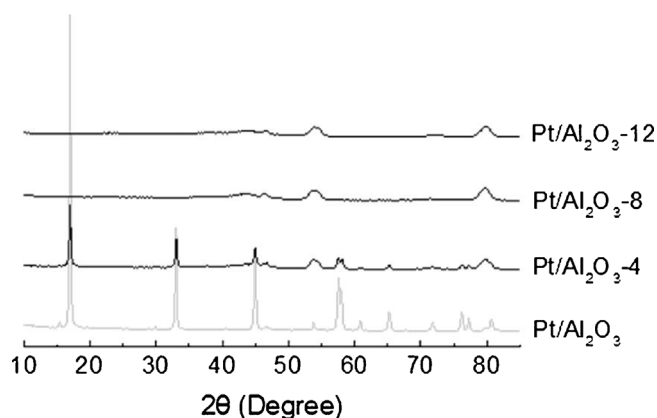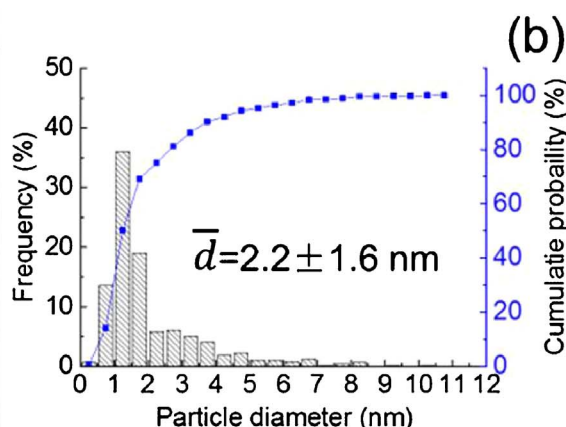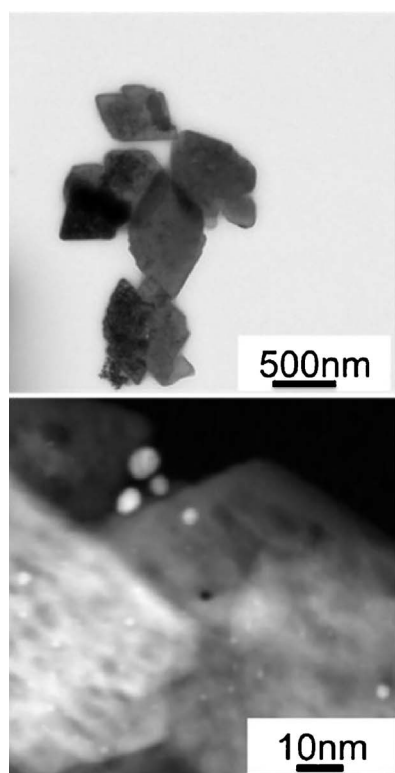**Fig. 5.** Product distributions from time course studies for (a) Pt/Al_2O_3, (b) Pt/Al_2O_3-4, (c) Pt/Al_2O_3-8 and (d) Pt/Al_2O_3-12.

Fig. 6. XRD patterns of spent overcoated as well as non-modified catalysts after 12 h of APR reaction.

2θ = 16.8°, 32.9°, 44.9°, 57.5° and 57.9°, which correspond to the (020), (120), (140), (031), (051) and (200) crystal planes of boehmite, respectively [23,27]. Boehmite formation was also seen for Pt/Al$_2$O$_3$-4, albeit to a much lesser extent given the low intensity and broadness of the boehmite diffraction peaks. In contrast, no sign of crystalline boehmite was detected in the XRD patterns of the samples that were overcoated for 8 and 12 h. This clearly shows that, depending on the degree of modification, boehmite formation can be slowed down or prevented. As mentioned above, the support phase transformation should lead to a severe loss of surface area. Indeed, an 86% decrease in surface area was observed for the spent non-modified catalyst (Table S2), in line with the XRD results. Additionally, this decrease is associated with a significant decrease of pore volume (Table S2). The surface area of spent Pt/Al$_2$O$_3$-4 increased remarkably up to 69 m^2/g, which is attributed to surface pitting, as a result of small boehmite particle formation [57]. Conversely, there was no significant drop in surface area seen for the 8 h overcoated sample.

STEM images of the Pt/Al$_2$O$_3$ and Pt/Al$_2$O$_3$-8 spent catalysts

corroborate the differences seen by XRD and N$_2$ physisorption (Fig. 7). After 12 h of APR reaction, flake-like boehmite patches are seen for Pt/Al$_2$O$_3$ catalyst, with sharp edges suggesting crystallinity. Large black clusters, identified by an Energy dispersive X-ray (EDX) line scan as Pt (Fig. S6), show that significant metal sintering happened during the APR process along with the support transformation. In stark contrast, no obvious differences in support morphology are seen for the 8 h overcoated sample before and after reaction. Some minor sintering did occur, though, with the mean particle size increasing from 1.5 ± 1.1–2.2 ± 1.6 nm for the spent Pt/Al$_2$O$_3$-8 sample, similar to previous observations in which metal sintering was eliminated in the present of protective layers deposited by atomic layer deposition or liquid-phase methods [58–61].

The TGA profiles of spent catalysts after 12 h APR reaction are shown in Fig. S7. The TGA traces can be roughly divided into 4 temperature regions based on the differential TGA analysis (Table S3). Weight loss between 50–180 °C is attributed to removal of adsorbed water. The second weight loss event occurs at 180–390 °C due to the desorption of interstitial H$_2$O and/or the desorption or decomposition of any adsorbed carbon-containing species, including carbonaceous deposits [62]. In the third temperature range of 390–650 °C, weight loss is normally attributed to water release due to the dehydration that occurs upon the phase transition of the support from boehmite back to γ-Al$_2$O$_3$ [63]. Weight loss at temperatures above 650 °C may be assigned to dehydroxylation of the support [21]. The weight loss in the temperature range from 390 to 650 °C, indicative for the extent of boehmite formation, drops with increasing modification time, with only 0.9% weight loss being detected for the spent Pt/Al$_2$O$_3$-12 specimen, compared to 14.6% for the non-modified sample. Besides, there is no weight loss in the temperature range of 180–390 °C for ethanol-washed Pt/Al$_2$O$_3$, indicating that carbonaceous deposits do not contribute to the deactivation seen for Pt/Al$_2$O$_3$.

Boehmite formation was further quantified by ^{27}Al MAS NMR spectroscopy, with the boehmite fraction being determined by linear combination of the spectra of γ-Al$_2$O$_3$ and boehmite. The NMR spectrum of spent Pt/Al$_2$O$_3$ exhibited only octahedrally coordinated

Fig. 7. STEM images of spent (a) Pt/Al$_2$O$_3$ and (b) Pt/Al$_2$O$_3$-8.

Table 3
Summary of boehmite formation characteristics for spent and recycled catalysts, as determined by ^{27}Al NMR.

		Octahedral Al species (%)	Tetrahedral Al species (%)	Boehmite fraction (%)
Pt/Al$_2$O$_3$	Fresh	67	33	0
	Spent	100	0	100
Pt/Al$_2$O$_3$-8	Fresh	68	32	0
	Spent	70	30	6
	Recycle 1	69	38	4
	Recycle 2	71	29	10
	Recycle 4	84	16	51

aluminum, suggesting quantitative conversion of the alumina support (Fig. 2 and Table 3) into boehmite [64]. In contrast, the octahedrally coordinated aluminum fraction in Pt/Al$_2$O$_3$-8 increased slightly from 68% to 70%, indicating that only 6% of the Al nuclei were present as boehmite. A previous study demonstrated that the formation of organic acids can have a negative effect on alumina catalyst stability [65]. In our case, the total yield of organic acids (LA + AA) is higher for overcoated catalysts than for the parent catalyst. This again suggests that surface silica deposition does indeed increase the hydrothermal stability of the catalyst, with the Pt/Al$_2$O$_3$-8 sample showing the best results in terms of activity and stability.

3.3. Catalyst activity and stability upon recycling

The hydrolytic stability of Pt/Al$_2$O$_3$-8 catalysts was further evaluated by reusing this catalyst. Normalized H$_2$ production rates are given to compare catalytic activity after reusing the catalyst several times. Obviously, H$_2$ production was inhibited completely for non-modified Pt/Al$_2$O$_3$ catalyst after first use (Fig. 8a). In contrast, Pt/Al$_2$O$_3$-8 showed essentially the same hydrogen productivity profile for the first reuse (Fig. 8b). Interestingly, upon second reuse, a clear increase in H$_2$ production rate was observed, showing a profile similar to the fresh, non-modified Pt/Al$_2$O$_3$ sample. Upon further recycling, hydrogen productivity drops greatly, with essentially no hydrogen being produced in the fourth recycle run. These results thus show that catalyst lifetime could be prolonged from 12 to 36 h, but also that deactivation, presumably by removal of the protective layers by Si−O−Si and Si−O−Al bond hydrolysis and eventually boehmite formation, ultimately does occur.

The spent Pt/Al$_2$O$_3$-8 catalyst recovered after recycling was characterized by various physicochemical techniques. The XRD patterns clearly show that the spent catalyst after the first recycle still did not exhibit any evidence for the formation of new crystalline structures (Fig. 9). However, after the second reuse, the first evidence of boehmite formation was seen, with boehmite peaks increasing in intensity upon further recycling.

^{27}Al NMR spectroscopic analysis of the reused catalysts provided insight into the extent of boehmite formation upon recycling (Fig. S8 and Table 3). The amount of octahedrally coordinated aluminum in the spent catalysts recovered the first and second recycle were 69% and 71%, corrending to 4% and 10% boehmite formation, respectively. However, the octahedrally coordinated aluminum fraction increased greatly to 84% after the fourth recycle, indicating that 51% of the support had transformed. In accordance with NMR analysis, the weight loss in the temperature range of 180–390 °C from TGA analysis of re-used catalysts showed similar changes (Fig. S9 and Table S5). Compared to the fresh Pt/Al$_2$O$_3$-8 catalyst, little variation was observed for the surface area of the spent catalysts during the original reaction and the first recycle (Table S4). However, the surface area of spent Pt/Al$_2$O$_3$-8 after the second recycle increased remarkably up to 66 m^2/g, which is comparable to that of the fresh non-modified catalyst. This surface area increase is attributed to surface pitting, as a result of small
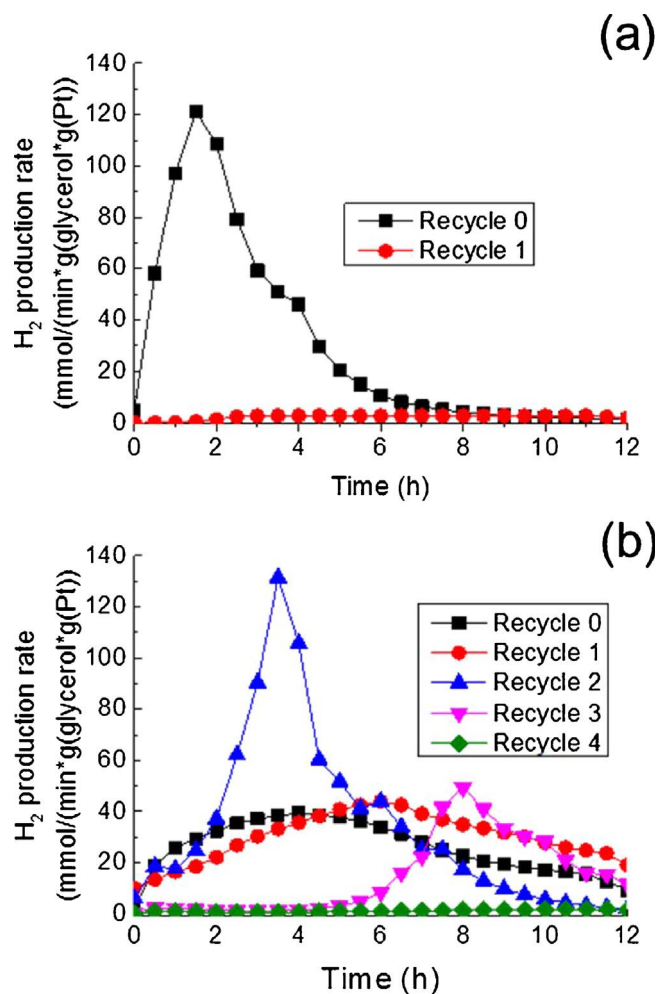
Fig. 8. H$_2$ production rate as function of time for different recycle tests of (a) Pt/Al$_2$O$_3$ and (b) Pt/Al$_2$O$_3$-8.
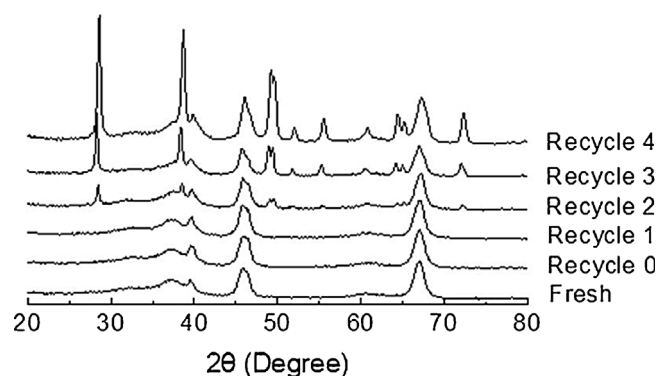

Fig. 9. XRD patterens of fresh Pt/Al$_2$O$_3$-8 and spent Pt/Al$_2$O$_3$-8 from recycle 0–4, respectively.

boehmite particle formation [57]. After that, the surface area of the spent catalyst decreased again due to structural collapse of alumina support, consistent with the transformation observed by XRD and NMR.

STEM analysis of the re-used catalysts (Fig. 10) showed the mean size of Pt particles in Pt/Al$_2$O$_3$-8 to increase from 1.5 nm for the fresh catalyst to 2.5, 3.7 and 4.4 nm for the spent catalyst after the first, second and fourth recycle, respectively. The spent Pt/Al$_2$O$_3$-8 catalyst obtained after the first and second recycles showed morphologies similar to the fresh sample (Fig. 10). However, after the fourth recycle, clear differences in the morphology of the alumina support can be seen.
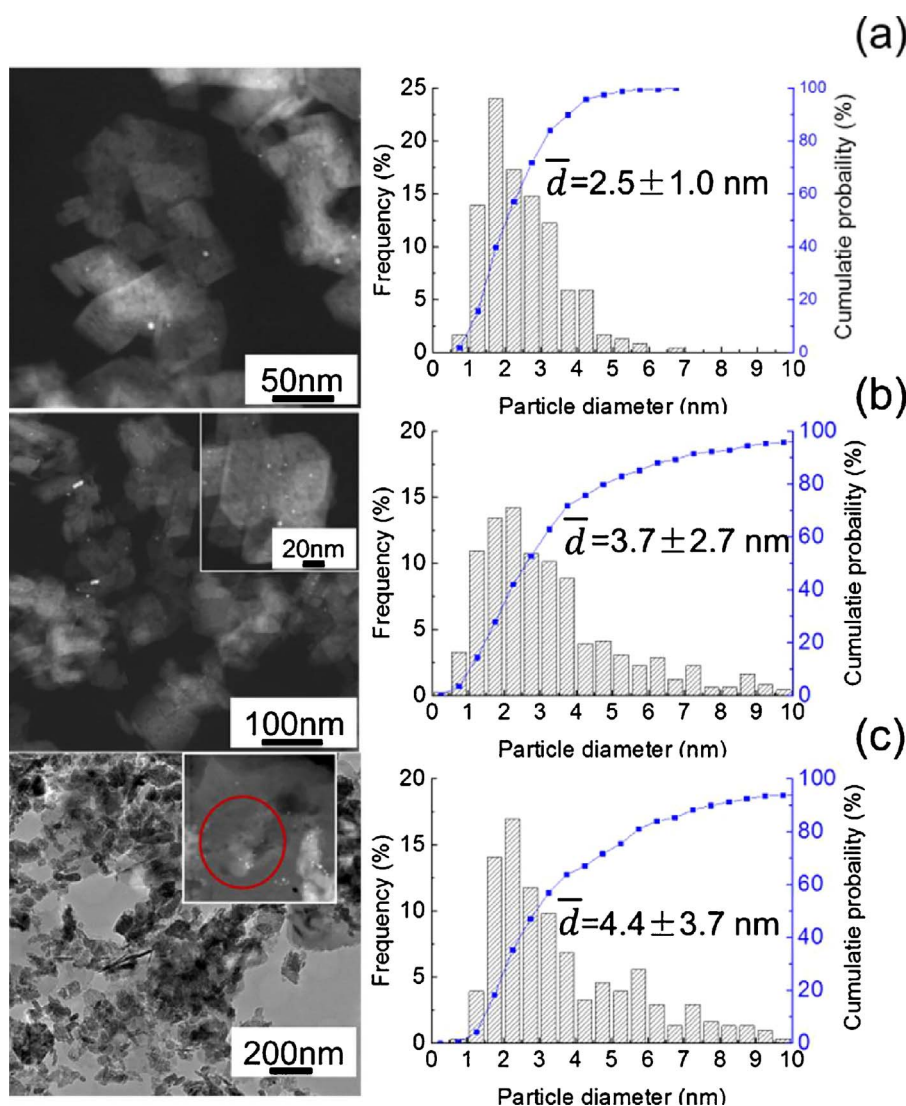
Fig. 10. STEM images and the corresponding particle size distribution for spent Pt/Al$_2$O$_3$-8 from (a) 1st recycle, (b) 2nd recycle and (c) 4th recycle.

Specifically, the amorphous alumina phase of the fresh catalyst changed to flake-like boehmite patches. In addition, the Pt particles and bulk alumina phase seem enveloped by a thin layer (red circle in Fig. 10c). The STEM images are consistent with previous studies that showed the encapsulation of metal particles by boehmite after APR reaction [66,67]. As a result of alumina phase collapse, the accessible metal surface area of Pt/Al$_2$O$_3$-8 decreased by 60% from 0.47 m^2/g to 0.19 m^2/g after the fourth recycle. ICP-OES analysis of the solution after reaction did not show any Pt leaching, but low concentrations of silicon were detected upon recycling (Table S4). Evidently, the deposited silica species are gradually hydrolyzed from the support under APR conditions, as a result of Si—O bond cleavage due to the nucleophilic attack of water [68]. Taken together, the results suggest that even though surface silica deposition is not a permanent solution against catalyst deactivation during reactions in hot liquid water, it does have a positive effect on catalyst lifetime.

4. Conclusion

We show that the hydrothermal stability of Pt/Al$_2$O$_3$ is enhanced by silylation, followed by calcination and reduction with tetraethylorthosilicate as silicon source. Catalyst characterization shows that silica deposition does not significantly alter the catalyst parent morphology, but results in a partial coverage of the active platinum phase. Silica deposition on Pt/Al$_2$O$_3$ rather than the bare support is preferred,

as controlled Pt deposition on silica-containing Al$_2$O$_3$ is difficult. FT-IR analysis shows that Al—O—Si bonds are generated at the expense of specific surface Lewis acid sites of the alumina support, giving rise to the generation of Brønsted acid sites. Total acidity, however, is found to decrease upon surface modification. As a result of Brønsted acid site formation and partial Pt blockage, the catalytic activity for APR of glycerol, as evidenced by the H$_2$ production rates, decreases upon modification. Based on XRD, STEM, ^{27}Al NMR and TGA characterization of the (recycled) catalysts, silica modification is shown to retard the support transformation process significantly. An 8 h overcoating treatment increases the lifetime of the catalyst three times from 12 to 36 h compared to the non-modified catalyst. These results clearly show that silica deposition can considerably improve catalyst stability in polar aqueous media, but also that more efficient methods of anchoring protective layers are needed.

technical support.

Appendix A. Supplementary data

Supplementary material related to this article can be found, in the online version, at doi:https://doi.org/10.1016/j.apcata.2017.11.025

References

[1] J.Q. Bond, A.A. Upadhye, H. Olcay, G.A. Tompsett, J.J.R. Xing, D.M. Alonso, D. Wang, T. Zhang, R. Kumar, A. Foster, S.M. Sen, C.T. Maravelias, R. Malina, S.R.H. Barrett, R. Lobo, C.E. Wyman, J.A. Dumesic, G.W. Huber, Energy Environ. Sci. 7 (2014) 1500–1523.
[2] D.M. Alonso, J.Q. Bond, J.A. Dumesic, Green Chem. 12 (2010) 1493–1513.
[3] G.W. Huber, J.A. Dumesic, Catal. Today 111 (2006) 119–132.
[4] M.C. Kim, T.W. Kim, H.J. Kim, C.U. Kim, J.W. Bae, Renew. Energy 95 (2016) 396–403.
[5] N.D. Subramanian, J. Callison, C.R.A. Catlow, P.P. Wells, N. Dimitratos, Int. J. Hydrog. Energy 41 (2016) 18441–18450.
[6] G. Wen, Y. Xu, H. Ma, Z. Xu, Z. Tian, Int. J. Hydrog. Energy 33 (2008) 6657–6666.
[7] N.H. Tran, G.S.K. Kannangara, Chem. Soc. Rev. 42 (2013) 9454–9479.
[8] A. Seretis, P. Tsiakaras, Renew. Energy 85 (2016) 1116–1126.
[9] M. Pagliaro, R. Ciriminna, H. Kimura, M. Rossi, C. Della Pina, Angew. Chem. Int. Ed. 46 (2007) 4434–4440.
[10] J.J. Bozell, G.R. Petersen, Green Chem. 12 (2010) 539–554.
[11] C.H. Zhou, H. Zhao, D.S. Tong, L.M. Wu, W.H. Yu, Catal. Rev. 55 (2013) 369–453.
[12] Y.C. Lin, Int. J. Hydrog. Energy 38 (2013) 2678–2700.
[13] A. Ciftci, D.A.J.M. Ligthart, E.J.M. Hensen, Green Chem. 16 (2014) 853–863.
[14] I. Coronado, M. Stekrova, M. Reinikainen, P. Simell, L. Lefferts, J. Lehtonen, Int. J. Hydrog. Energy 41 (2016) 11003–11032.
[15] R.R. Davda, J.A. Dumesic, Chem. Commun. 10 (2004) 36–37.
[16] T. Nozawa, Y. Mizukoshi, A. Yoshida, S. Naito, Appl. Catal. B Environ. 146 (2014) 221–226.
[17] R.R. Davda, J.W. Shabaker, G.W. Huber, R.D. Cortright, J.A. Dumesic, Appl. Catal. B Environ. 43 (2003) 13–26.
[18] C. Chizallet, P. Raybaud, Catal. Sci. Technol. 4 (2014) 2797–2813.
[19] J.P. Lange, Angew. Chem. Int. Ed. 54 (2015) 13187–13197.
[20] F. Héroguel, B. Rozmysłowicz, J.S. Luterbacher, Chimia 69 (2015) 582–591.
[21] G. Lefèvre, M. Duc, P. Lepeut, R. Caplain, M. Fédoroff, Langmuir 18 (2002) 7530–7537.
[22] D.D. MacDonald, P. Butler, Corros. Sci. 13 (1973) 259–274.
[23] R.M. Ravenelle, J.R. Copeland, W.G. Kim, J.C. Crittenden, C. Sievers, ACS Catal. 1 (2011) 552–561.
[24] C. Sievers, Y. Noda, L. Qi, E.M. Albuquerque, R.M. Rioux, S.L. Scott, ACS Catal. 6 (2016) 8286–8307.
[25] J.R. Copeland, X.R. Shi, D.S. Sholl, C. Sievers, Langmuir 29 (2013) 581–593.
[26] R.M. Ravenelle, J.R. Copeland, A.H. Van Pelt, J.C. Crittenden, C. Sievers, Top. Catal. 55 (2012) 162–174.
[27] A.L. Jongerius, J.R. Copeland, G.S. Foo, J.P. Hofmann, P.C.A. Bruijnincx, C. Sievers, B.M. Weckhuysen, ACS Catal. 3 (2013) 464–473.
[28] M. Absi-Halabi, A. Stanislaus, H. Al-Zaid, Appl. Catal. A Gen. 101 (1993) 117–128.
[29] B.C.O.R. Espinoza, K. Jothimurugesan, Y. Jin, J. Ortego, K. Fjare, Stabilized boehmite-derived catalyst supports, catalysts, methods of making and using, US 20080039539 A1 (2007).
[30] O.P.Y. Jin, R.L. Espinoza, N. Srinivasan, Ionkina, Stabilized transition alumina catalyst support from boehmite and catalysts made therefrom, US7402612 B2 (2003).
[31] A.J. Byrd, R.B. Gupta, Appl. Catal. A Gen. 381 (2010) 177–182.
[32] H.N. Pham, A.E. Anderson, R.L. Johnson, K. Schmidt-Rohr, A.K. Datye, Angew. Chem. Int. Ed. 51 (2012) 13163–13167.
[33] H. Xiong, T.J. Schwartz, N.I. Andersen, J.A. Dumesic, A.K. Datye, Angew. Chem. Int. Ed. 54 (2015) 7939–7943.
[34] M.C. Capel-Sanchez, L. Barrio, J.M. Campos-Martin, J.L.G. Fierro, J. Colloid Interface Sci. 277 (2004) 146–153.
[35] A.M. Fidalgo, L.M. Ilharco, Microporous Mesoporous Mat. 158 (2012) 39–46.
[36] L.A.S.A. Prado, M. Sriyai, M. Ghislandi, A. Barros-Timmons, K. Schulte, J. Braz. Chem. Soc. 21 (2010) 2238–2245.
[37] P.A. Zapata, J. Faria, M.P. Ruiz, R.E. Jentoft, D.E. Resasco, J. Am. Chem. Soc. 134 (2012) 8570–8578.
[38] S. Sato, R. Takahashi, T. Sodesawa, D. Shin, N. Ichikawa, K. Ogura, Bull. Chem. Soc. Jpn. 79 (2006) 649–655.
[39] A.G. Shastri, J. Schwank, J. Catal. 95 (1985) 271–283.
[40] J. Datka, J. Catal. 135 (1992) 186–199.
[41] W. Lin, A.A. Herzing, C.J. Kiely, I.E. Wachs, J. Phys. Chem. C 112 (2008) 5942–5951.
[42] M. Williams, B. Fonfe, C. Sievers, A. Abraham, J. Vanbokhoven, A. Jentys, J. Vanveen, J. Lercher, J. Catal. 251 (2007) 485–496.
[43] D. Huang, M. Ke, X. Bao, H. Liu, Ind. Eng. Chem. Res. 55 (2016) 1192–1201.
[44] A.R. Mouat, C. George, T. Kobayashi, M. Pruski, R.P. van Duyne, T.J. Marks, P.C. Stair, Angew. Chem. Int. Ed. 54 (2015) 13346–13351.
[45] C.A. Emeis, J. Catal. 141 (1993) 347–354.
[46] M. Digne, P. Sautet, P. Raybaud, P. Euzen, H. Toulhoat, J. Catal. 211 (2002) 1–5.
[47] T. Armaroli, T. Bécue, S. Gautier, Oil Gas Sci. Technol. 59 (2004) 215–237.
[48] G. Busca, V. Lorenzelli, G. Ramis, R.J. Willey, Langmuir 9 (1993) 1492–1499.
[49] E. Brunner, Catal. Today 38 (1997) 361–376.
[50] M. Guisnet, P. Andy, N.S. Gnep, C. Travers, E. Benazzi, Progress in Zeolite and Microporous Materials, 1st ed., Elsevier, Amsterdam, 1996.
[51] G.W. Huber, J.W. Shabaker, S.T. Evans, J.A. Dumesic, Appl. Catal. B Environ. 62 (2006) 226–235.
[52] D.A. Boga, R. Oord, A.M. Beale, Y.M. Chung, P.C.A. Bruijnincx, B.M. Weckhuysen, ChemCatChem 5 (2013) 529–537.
[53] A. Wawrzetz, B. Peng, A. Hrabar, A. Jentys, A.A. Lemonidou, J.A. Lercher, J. Catal. 269 (2010) 411–420.
[54] R.D. Cortright, R.R. Davda, J.A. Dumesic, Nature 418 (2002) 964–967.
[55] A. Ciftci, B. Peng, A. Jentys, J.A. Lercher, E.J.M. Hensen, Appl. Catal. A Gen. 431–432 (2012) 113–119.
[56] R. Weingarten, G.A. Tompsett, W.C. Conner, G.W. Huber, J. Catal. 279 (2011) 174–182.
[57] H. Xiong, H.N. Pham, A.K. Datye, Green Chem. 16 (2014) 4627–4643.
[58] J.W. Han, C. Kim, J.S. Park, H. Lee, ChemSusChem 7 (2014) 451–456.
[59] J. Lu, B. Fu, M.C. Kung, G. Xiao, J.W. Elam, H.H. Kung, P.C. Stair, Science 335 (2012) 1205–1208.
[60] F. Héroguel, B.P. Le Monnier, K.S. Brown, J.C. Siu, J.S. Luterbacher, Appl. Catal. B Environ. 218 (2017) 643–649.
[61] B.J. O'Neill, D.H.K. Jackson, A.J. Crisci, C.A. Farberow, F. Shi, A.C. Alba-Rubio, J. Lu, P.J. Dietrich, X. Gu, C.L. Marshall, P.C. Stair, J.W. Elam, J.T. Miller, F.H. Ribeiro, P.M. Voyles, J. Greeley, M. Mavrikakis, S.L. Scott, T.F. Kuech, J.A. Dumesic, Angew. Chem. Int. Ed. 52 (2013) 13808–13812.
[62] M. El Doukkali, A. Iriondo, J.F. Cambra, I. Gandarias, L. Jalowiecki-Duhamel, F. Dumeignil, P.L. Arias, Appl. Catal. A Gen. 472 (2014) 80–91.
[63] M. El Doukkali, A. Iriondo, J.F. Cambra, P.L. Arias, Top. Catal. 57 (2014) 1066–1077.
[64] M. Trueba, S.P. Trasatti, Eur. J. Inorg. Chem. 2005 (2005) 3393–3403.
[65] D.J.M. de Vlieger, L. Lefferts, K. Seshan, Green Chem. 16 (2014) 864.
[66] K. Koichumanova, A.K.K. Vikla, D.J.M. de Vlieger, K. Seshan, B.L. Mojet, L. Lefferts, ChemSusChem 6 (2013) 1717–1723.
[67] D.J.M. de Vlieger, B.L. Mojet, L. Lefferts, K. Seshan, J. Catal. 292 (2012) 239–245.
[68] R.M. Ravenelle, F. Schüßler, A. D'Amico, N. Danilina, J.A. van Bokhoven, J.A. Lercher, C.W. Jones, C. Sievers, F. Schübler, A. Damico, N. Danilina, J.A. van Bokhoven, J.A. Lercher, C.W. Jones, C. Sievers, J. Phys. Chem. C 114 (2010) 19582–19595.